THE JOURNAL OF PHYSICAL CHEMISTRY LETTERS
A JOURNAL OF THE AMERICAN CHEMICAL SOCIETY

pubs.acs.org/JPCL

Letter

Growth of Clathrate Hydrates in Nanoscale Ice Films Observed Using Electron Diffraction and Infrared Spectroscopy

Bijesh K. Malla, Ding-Shyue Yang,* and Thalappil Pradeep*

Cite This: *J. Phys. Chem. Lett.* 2025, 16, 365−371

Read Online

ACCESS | Metrics & More | Article Recommendations | Supporting Information

ABSTRACT: Clathrate hydrates (CHs) are believed to exist in cold regions of space, such as comets and icy moons. While spectroscopic studies have explored their formation under similar laboratory conditions, direct structural characterization using diffraction techniques has remained elusive. We present the first electron diffraction study of tetrahydrofuran (THF) and 1,3-dioxolane (DIOX) CHs in the form of nanometer-thin ice films under an ultrahigh vacuum at cryogenic temperatures. Using reflection high-energy electron diffraction, we show that THF CH grows readily on various substrates during thermal annealing of an amorphous ice mixture of THF and water, and the formation is independent of the nature of the substrate. The growth of DIOX CHs on a Au(111) substrate is similar. A comparison of electron diffraction patterns with calculated X-ray diffraction patterns indicates that THF and DIOX form structure II CH ($5^{12}6^4$) with a lattice constant of ∼17.2 Å (cubic $Fd\bar{3}m$). Both CHs were also grown on Ru(0001) and were examined by reflection absorption infrared spectroscopy. A direct comparison of diffraction data to infrared spectra as a function of the temperature further demonstrates the strength of multiple probes in examining complex systems possessing diverse molecular interactions.

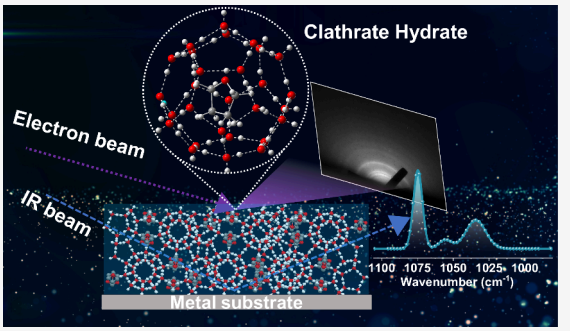

Existence of clathrate hydrates (CHs) in the simulated interstellar environment has been established by infrared spectroscopy.[1] CHs represent a unique class of compounds, where water molecules form cages to encapsulate guest molecules, creating crystalline solids. This molecular arrangement of water allows for the inclusion of a variety of molecules, such as CH_4, C_2H_6, C_3H_8, CO_2, N_2, O_2, and others, within the crystalline structures.[2] Typically, CHs exhibit three crystalline structures: structure I (sI, cubic $Pm\bar{3}n$), structure II (sII, cubic $Fd\bar{3}m$), and structure H (sH, hexagonal $P6/mmm$), and they generally occur under high-pressure conditions.[3−5] Since the detection of methane CH in 2019 at 30 K under ultrahigh-vacuum (UHV) conditions[6] principally using reflection absorption infrared spectroscopy (RAIRS), there have been several reports on the CHs of molecules. They include those of ethane (C_2H_6),[7] formaldehyde (HCHO),[8] acetone (CH_3COCH_3),[9] acetaldehyde (CH_3COH),[10] tetrahydrofuran [$(CH_2)_4O$],[11,12] and dimethyl ether (CH_3OCH_3).[13] The formation of CHs occurs typically starting from an amorphous ice mixture of the guest and host water molecules upon slow thermal annealing. It was noted in the original report that maintaining a methane/water mixture at 30 K for 25 h produces a characteristic methane CH peak at 3017 cm^{-1}, corresponding to the C−H stretch of CH_4 encaged in the 5^{12} cage. Deconvolution of this feature showed that 13% of total methane exists as CH under this condition. Since then, it has been possible to encage different percentages of guest molecules in CHs under different temperature conditions in UHV. CO_2, in particular, produces hydrate even at 10 K, for which the infrared spectrum was known in the literature.[14,15] Additionally, studies of interactions of low-energy electrons and photons with various caged molecules have been conducted in UHV, although these have not been explicitly assigned to CHs.[16−18]

A key question that comes up in such investigations is the independent confirmation of CHs by structural tools, especially using scattering techniques. As these experiments are conducted on thin films with thicknesses in the nanometer scale, a suitable option for structural characterization is electron diffraction.[19−21] Electron diffraction in a transmission electron spectroscope (of methanol CH) was reported in 1991, under 10^{-6} Torr.[14] However, no report exists in UHV on any of the hydrates at temperatures below 160 K, which is typically the desorption temperature of water in UHV conditions.[22] Considering the nature of RAIRS conducted on single-crystal surfaces, a natural choice for structural studies is reflection high-energy electron diffraction (RHEED). It is a well-suited technique for studying the structures and phase transitions of

Received: October 28, 2024
Revised: November 26, 2024
Accepted: December 6, 2024

https://doi.org/10.1021/acs.jpclett.4c03106
J. Phys. Chem. Lett. 2025, 16, 365−371

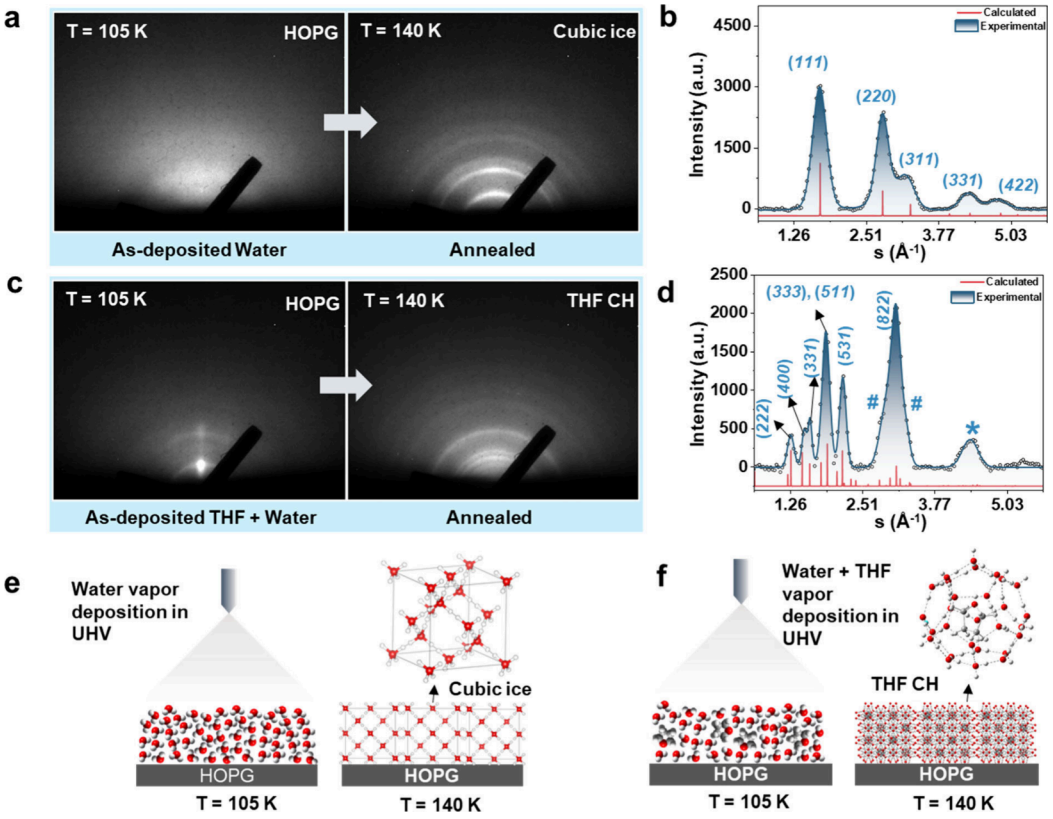

Figure 1. Evolution of ice Ic and THF CH explored with RHEED. (a) Electron diffraction images of as-deposited water on HOPG at 105 K and after annealing to 140 K. (b) Comparison of the experimental radially averaged electron diffractions of annealed water ice at 140 K with the calculated diffraction peaks (red lines) of ice Ic. (c) Electron diffraction images of the as-deposited THF−water ice mixture on HOPG at 105 K and after annealing to 140 K. (d) Comparison of the experimental radially averaged electron diffractions of annealed THF−water ice at 140 K with the calculated (red lines) diffraction peaks of sII THF CH. Peaks labeled with # are attributed to ice Ic, while that marked with ∗ corresponds to the collection of low-intensity signals of THF CH, shown in the theoretical spectrum. (e) Schematic diagram of the formation of ice Ic on HOPG from vapor-deposited ice. (f) Schematic diagram of the formation of sII THF CH on HOPG from vapor-deposited ice.

solid-supported molecular thin films, and our lab has conducted several experiments in this regard.[23−28] In the present work, we report the first RHEED experiment of tetrahydrofuran (THF, C_4H_8O) and 1,3-dioxolane (DIOX, $C_3H_6O_2$) CHs under UHV, and the results were compared to the simulated diffraction data. The emergence of CHs under the same temperature and pressure conditions was confirmed by RAIRS. Although THF and DIOX have not yet been detected in the interstellar medium (ISM), various similar molecules, such as dimethyl ether, propylene oxide, and ethylene oxide, have been identified.[29−31] Given the ongoing advancements in astronomical observations, the detection of THF and DIOX in the ISM may be possible in the near future. We believe that these investigations further enrich our understanding of the formation of CHs in UHV and cryogenic conditions and present opportunities for their exploration using other UHV techniques, such as low-energy ion scattering.[32,33] It is worth noting that, while the RHEED and RAIRS measurements were performed on separate instruments, both were conducted under identical temperature and pressure conditions to ensure consistency. For the RHEED experiments, ice films were grown on three distinct substrates: highly oriented pyrolytic graphite (HOPG, ZYA grade), single-crystalline Au(111) (Princeton Scientific), and a hydrophobic self-assembled monolayer (SAM) of 1-octadecanethiol on Au(111). Co-deposition methods were employed to create thin films of ice with an approximate thickness of 25 nm for CH preparation. This process involved the simultaneous deposition of premixed vapors of THF or DIOX with water for 10 min. For the RAIRS experiments, the Ru(0001) substrate was used to prepare thin ice films. A mixed ice film with an approximate thickness of 60 nm, composed of THF/DIOX and water in a 1:3 ratio, was prepared on the Ru(0001) substrate at 105 K. This was achieved by backfilling the chamber with THF/DIOX and water vapor for a duration of 10 min at a total pressure of 5×10^{-7} mbar. The experimental procedures and ice thickness calculations for both RHEED and RAIRS are detailed in the Supporting Information. Calculated X-ray diffraction (XRD) patterns are shown in panels b and d of Figure 1 for cubic ice (ice Ic, a = 6.35 Å)[34] and THF CH (a = 17.21 Å)[35] along with Figure S4 of the Supporting Information for hexagonal ice (ice Ih, a/b = 4.49 Å and c = 7.33 Å),[36] calculated using the VESTA software.[37] These patterns were compared to the experimental electron diffraction patterns to validate the phase identification.

In Figure 1, we present the evolution of ice Ic and CH of THF grown on HOPG in the temperature window of 105−140 K. Under high-vacuum (~10^{-6}−10^{-8} mbar) conditions, amorphous ice typically crystallizes into ice Ic, ice Ih, or stacking-disordered ice.[38−41] The crystal structure may be significantly influenced by the substrate and temperature.[20] Prior to investigating the formation of CH, we commenced our study with an examination of the structure of pure ice, as these are well-characterized by RHEED.[21,23] Figure 1a shows the

https://doi.org/10.1021/acs.jpclett.4c03106
J. Phys. Chem. Lett. 2025, 16, 365−371

Table 1. Electron Diffraction Results for Ice Ic, sII THF, and DIOX CH, with Calculated and Observed *hkl* (Crystallographic Indices) and *d* (Bragg Distance)[a]

cubic ice calculated		cubic ice observed	sll THF CH calculated		sll THF CH observed	sll DIOX CH observed
hkl	*d*	*d*	*hkl*	*d*	*d*	*d*
			111(s)	9.94		
			311(w)	5.19	5.10$	
			222(s)	4.97	4.98&	
			400(s)	4.30	4.31$	
			331(s)	3.94	3.93$	3.92
111(s)	3.67(s)	3.68				
			422(s)	3.51	3.50$	
			333/511(s)	3.31	3.30&	3.33&
			440(w)	3.04		
			531(s)	2.91	2.90	2.94
			620(w)	2.72		
			533(w)	2.62		
220(s)	2.24(s)	2.24	731(w)	2.24	2.21$	2.21$
			733(w)	2.02	2.02$	
			822/660(s)	2.02	2.03&	2.03&
			555/751(w)	1.98		
311(s)	1.91(s)	1.96			1.92$	1.92$
331(s)	1.45(s)	1.47				
422(s)	1.29(s)	1.29				

[a]Calculated *d* values (Å) are obtained using a = 6.35 Å for ice Ic and 17.21 Å for THF CH. The symbols & and $ represent the composite broad peak having a peak center at the *d* value shown and the peak that combines with a broad peak; s represents strong peak intensity; and w represents weak peak intensity.

RHEED images of as-deposited water ice on HOPG and after its annealing to 140 K. Amorphous solid water (ASW) of approximately 120 nm thickness was accumulated on the HOPG surface by vapor deposition of water under UHV conditions, as shown in Figure 1e. Diffuse scattering with broad ring-like features at 105 K (Figure 1a) indicates low-density ASW with only a short-range order for the as-deposited ice. After annealing to 140 K, sharper Debye−Scherrer rings emerge in the electron diffraction pattern, which indicates the crystallization of ASW into a randomly oriented polycrystalline specimen around 140 K (Figure 1a). This ring pattern is unchanged until the desorption of ice. Figure 1b presents a comparison between the experimental radially averaged electron diffraction intensity curves as a function of momentum transfer, $s = (4\pi/\lambda)\sin(\theta/2)$, where θ is the total angle of scattering, and the calculated XRD spectrum for ice Ic. The observed positions of the (111), (220), (311), (331), and (442) electron diffraction peaks of ice Ic match well with the calculated values, indicating the formation of ice Ic with a lattice constant of a = 6.35 Å.[23,34,42] The large diffraction width is the result of a finite crystallite size of a few nanometers on average, estimated according to the Scherrer formula.[23]

To create THF CH, THF−water mixed vapor was co-deposited on the HOPG substrate at 105 K and then annealed to higher temperatures (panels c and f of Figure 1). At 105 K (Figure 1c), the observation of electron diffraction spots and diffuse ring patterns suggests the formation of crystalline THF in ASW. This may be understood because vapor deposition of pure THF on HOPG at 105 K results in a RHEED pattern of clear electron diffraction spots without rings, which signifies an ordered crystalline phase with respect to the supporting surface (Figure S1 of the Supporting Information). Additionally, the RAIRS study showed that THF undergoes a phase transition from an amorphous assembly to a crystalline phase near 90 K (Figure S2 of the Supporting Information). Upon thermal annealing of the ice mixture to 140 K, the initial electron diffraction spots disappear and new Debye−Scherrer rings emerge, which are substantially different from those of ice Ic (panels b and d of Figure 1). Concurrently, during the thermal annealing process, an increase in the chamber pressure was noted, indicating the partial desorption of THF from the water ice matrix, as evidenced by the gradual disappearance of the electron diffraction spots (Figure S3 of the Supporting Information). The loss of THF from the ice matrix during annealing was again confirmed by the RAIRS study (Figure 4). This desorption as a result of increased mobility likely facilitates intermolecular motions of THF, leading to the formation of THF CH.

Radially averaged electron diffraction intensities were calculated from the RHEED image of Figure 1b at 140 K and were compared to the calculated diffraction peaks for sII THF CH.[31] Agreement of the positions of high-intensity peaks is satisfactory, which signifies the presence of sII THF CH with a cubic lattice of a = 17.2 Å.[35,43] The relatively smaller peaks corresponding to the (220) and (311) diffractions of ice Ic were noted (marked by # in Figure 1d), suggesting a minor fraction of ice Ic within the thin film. For clarity, a comparison of the observed and calculated interplanar distances of ice Ic and THF CH is provided in Table 1. The possible presence of ice Ih contributing to the stacking disorder was also considered, and a comparison of the calculated diffraction patterns of ice Ic, ice Ih, and THF CH against the experimental electron diffraction of THF CH is provided in Figure S4 of the Supporting Information. Although stacking faults are present, their occurrence is expected to be minimal in polycrystalline ice.

The formation of ice Ic and ice Ih significantly depends upon the substrate structure, as shown in the literature,[19,20] but the emergence of CH is independent of the substrates used for deposition. This was established by conducting the same

https://doi.org/10.1021/acs.jpclett.4c03106
J. Phys. Chem. Lett. 2025, 16, 365−371

experiments on two other substrates: Au(111) and a SAM of 1-octadecanethiol on Au(111), a hydrophobic surface. The electron diffraction streaks seen in the top row of Figure 2

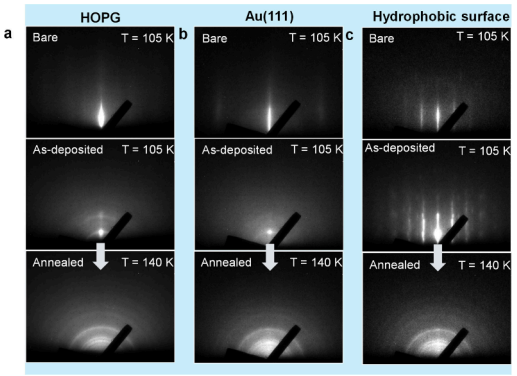

Figure 2. Evolution of THF CH on HOPG, Au(111), and the hydrophobic surface [SAM of 1-octadecanethiol on Au(111)]. The RHEED images, displayed vertically, show (a) bare HOPG, (b) Au(111), and (c) a hydrophobic surface at 105 K (top row), the as-deposited THF−water ice mixture on the respective substrate at 105 K (middle row), and the same ice mixture on the respective substrate after annealing at 140 K (bottom row).

correspond to the ordered structures of the bare surfaces.[44] Evidently, the same ring pattern was obtained at 140 K (bottom row of Figure 2), indicating CH formation on these substrates, even though the initial thin-film structures may exhibit differences (middle row of Figure 2). This confirmed that, regardless of the interface, THF and water formed CH around 140 K.

To examine the preference of CH formation under UHV conditions, we conducted experiments with DIOX, another guest for stable CHs. To create DIOX CH, a mixed vapor of DIOX−water was deposited on the Au(111) substrate at 105 K and annealed to 140 K. At 105 K, the diffused RHEED pattern seen from the as-deposited mixture of DIOX and water molecules indicates the largely amorphous nature of the ice mixture. The electron diffraction spots suggest the formation of DIOX crystallites, as noted in Figure 1c. After annealing to 140 K, the same Debye−Scherrer rings appeared as in the case of THF CH (Figure 3a). The experimental and calculated Bragg diffractions and their corresponding interplanar distances are compared in Table 1. Here, it is worth noting that the experimentally obtained electron diffraction pattern of DIOX CH is compared to the calculated XRD pattern of THF CH due to the unavailability of the crystallographic information file (CIF) for DIOX CH. DIOX is known to form sII CH under high-pressure conditions and has a lattice constant similar to that of THF,[43] with comparable van der Waals radii (THF, 2.95 Å; DIOX, 2.8 Å).[45] XRD patterns of CHs formed by different molecules are comparable if they adopt the same hydrate structure.[3] This comparability has been utilized in selected area electron diffraction studies of methanol CH, with ethanol and THF, as they all form sII CH.[14] In our study, we note that the positions of the (331), (333)/(511), (531), and (822) electron diffractions match well with the calculated peaks of sII THF CH. Additionally, the formation of a minor fraction of ice Ic was confirmed by the presence of the (220) and (311) intensities (Figure 3b). These electron diffraction results confirm the successful formation of sII CH of DIOX at 140 K in UHV.

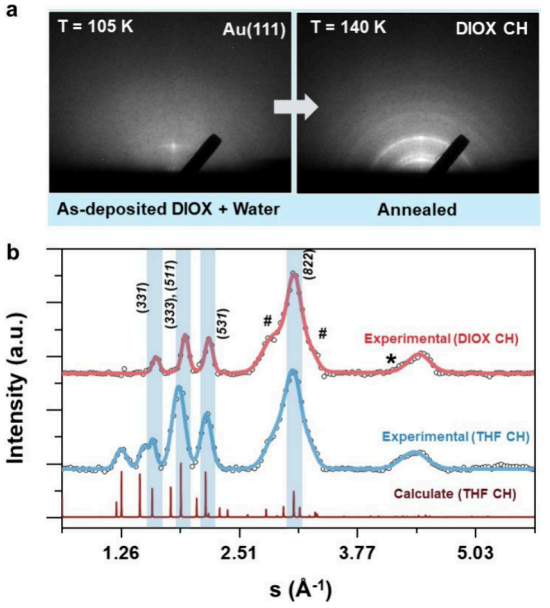

Figure 3. CH formation of DIOX was studied using RHEED. (a) Diffraction images of as-deposited water on the DIOX substrate at 105 K and after annealing to 140 K. (b) Experimental radially averaged diffraction pattern of annealed DIOX−water ice and that of annealed THF−water ice, both at 140 K, compared to the calculated diffraction pattern of sII THF CH. Peaks labeled with # are attributed to ice Ic, while that marked with ∗ corresponds to the collection of low-intensity signals of DIOX CH, shown in theoretical THF CH.

The formation of CHs of THF and DIOX was further investigated using RAIRS. To form the CH, vapors of THF and water were co-deposited on a Ru(0001) substrate at 105 K and annealed to 140 K with a ramping rate of 2 K/min. Figure 4a shows the RAIR spectra of the THF−water ice mixture at 105 and 140 K in the C−O antisymmetric stretching region of THF. The RAIR spectrum at 105 K shows three peaks at 1053, 1032, and 1013 cm^{-1} and a weak broad peak around 1069 cm^{-1}, which are attributed to different fractions of THF trapped in ASW, with different hydrogen-bonding structures of the ice matrix. After annealing to 140 K, a new peak emerges at 1074 cm^{-1}, which is attributed to THF trapped in the large cage ($5^{12}6^4$) of sII CH. From the RAIR spectrum, it is evident that there is some uncaged THF remaining in the matrix at 140 K. The decrease in the band area of the RAIR spectra after annealing indicates the loss of THF due to its desorption. Analysis of the band areas revealed that only 17.4% of the total deposited THF forms CH, while 16.5% remains uncaged in the ice matrix, and 66.1% desorbs. In Figure 4c, the temperature-dependent evolution of the THF CH is shown. THF CH formation started around 130 K, and the fraction kept on increasing until 150 K.

For the formation of DIOX CH, DIOX and water vapors were co-deposited on the Ru(0001) substrate at 105 K and annealed to 140 K. Figure 4b shows the RAIR spectra of the DIOX−water ice mixture at 105 and 140 K in the C−O ring stretching region. At 105 K, the peak at 1027 cm^{-1} indicates amorphous DIOX, trapped in ASW; the same peak was compared to pure amorphous DIOX (Figure S5 of the Supporting Information). Upon annealing to 140 K, a new peak emerged at 1036 cm^{-1} (Figure 4b), indicating the formation of DIOX CH, where DIOX molecules were trapped in the $5^{12}6^4$ cages of the sII hydrate structure. Simultaneously,

https://doi.org/10.1021/acs.jpclett.4c03106
J. Phys. Chem. Lett. 2025, 16, 365−371

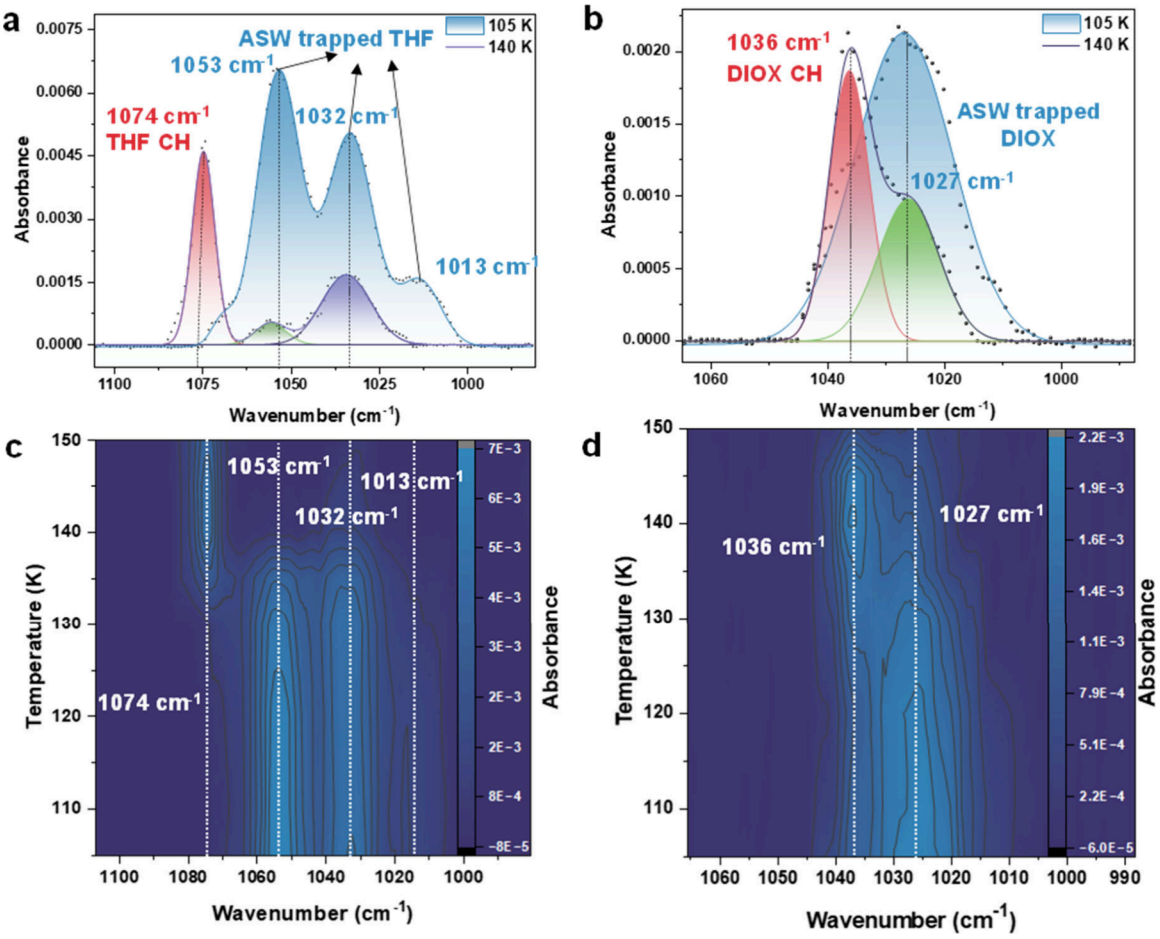

Figure 4. CH formation of THF and DIOX studied by RAIR spectroscopy. (a) RAIR spectra of the THF−water ice mixture in the C−O antisymmetric stretching region of THF at 105 and 140 K, respectively. At 140 K, the RAIR spectrum is deconvoluted into three components, highlighted in red (1074 cm^{-1}), green (1053 cm^{-1}), and violet (1032 cm^{-1}) colors. (b) RAIR spectra of the DIOX−water ice mixture in the C−O ring stretching region of DIOX at 105 and 140 K, respectively. At 140 K, the RAIR spectrum is deconvoluted into two components, highlighted in red (1036 cm^{-1}) and green (1027 cm^{-1}) colors. Temperature-dependent evolution of different peaks in the (c) C−O antisymmetric stretching region of THF in the THF−water ice mixture and (d) C−O ring stretch stretching region of DIOX in the DIOX−water ice mixture.

there was a notable decrease in the peak intensity at 1027 cm^{-1}, corresponding to trapped DIOX in the ice matrix. The observed blue shift in the peak position is attributed to the interaction between DIOX molecules and the host hydrate cages, reflecting a change in the molecular environment. Deconvolution of the RAIR spectrum at 140 K revealed that 35% of DIOX forms CH, while 28% remains uncaged within the ice matrix from the total deposited DIOX molecules. In Figure 4d, the temperature-dependent evolution of DIOX CH is shown, where DIOX CH started growing at 130 K. The electron diffraction data (Figures 1 and 3) showed the formation of sII CH of THF and DIOX. The infrared (IR) results provide evidence for the formation of $5^{12}6^4$ cages of sII. We note that, while RHEED provides structural details of the topmost monolayers, RAIRS offers information about the entire thin film of ice. From the above results, it is evident that CH formation is facile in a nanometer-thin amorphous ice mixture in UHV conditions at a suitable temperature where the intermolecular mobility is high. The formation of CHs on different substrates proved that the structure of the interface did not significantly affect the nucleation of CHs.

The nucleation of CHs in amorphous solids can be classified as homogeneous nucleation due to the absence of any observable surface effects.[5] Under high-pressure conditions, two intermediate pathways are predicted for CH nucleation, theoretically.[46] One pathway follows the crystalline critical nucleus, while the other involves an amorphous critical nucleus as an intermediate step before transitioning into crystalline CH. Specifically, in the case of amorphous critical nucleation, a metastable amorphous CH is initially formed, which requires an additional activation barrier to convert into its crystalline form.[5,46−48] In our system, starting with an amorphous mixture of water and guest molecules, the formation of a critical amorphous nucleus may be favored, which, with an increase in the temperature, results in the crystallization of CHs. Our previous study demonstrated that, at 120 K, the majority of THF forms CHs after a 110 h incubation period, which is significantly reduced to 6 h at 135 K; however, the current RHEED results indicate that, at 140 K, CH formation occurs rapidly, with a minimal time required for nucleation. The activation energy for this process was found to be 23.12 kJ mol^{-1}, lower than that required for the crystallization of ASW.[8] On the basis of these findings, we propose that CH formation under UHV conditions likely follows the amorphous critical nucleation pathway. In this scenario, some molecules forming metastable amorphous CHs may fail to crystallize and will subsequently decompose into either ice Ic or ice Ih.[9,10,13] To validate this suggestion, nucleation at the molecular level may

https://doi.org/10.1021/acs.jpclett.4c03106
J. Phys. Chem. Lett. 2025, 16, 365−371

be examined using cryo-electron microscopy, and we will be pursuing this in the future.

The data presented in this study confirmed the formation of CHs under UHV conditions under cryogenic temperatures, as evidenced by RAIRS and RHEED data. Both THF and DIOX demonstrated the formation of CHs upon gradual thermal annealing around 140 K, where the intermolecular motion of water becomes possible. The RHEED data were compared to the available XRD data. This CH formation was shown to be substrate-independent, as similar results were obtained on HOPG, Au(111), and a hydrophobic SAM substrate. While this study specifically focuses on two guest molecules, a direct comparison of electron diffraction data with IR spectra of several CHs would expand the scope of this research, facilitating the study of diverse molecular interactions in cryogenic conditions. The confirmation of CH formation by electron diffraction and spectroscopy on different substrates may offer additional support for their existence in space.

■ ASSOCIATED CONTENT

Supporting Information

The Supporting Information is available free of charge at https://pubs.acs.org/doi/10.1021/acs.jpclett.4c03106.

Experimental section, RHEED images of pure THF, electron diffraction spectra, and RAIRS of pure THF and DIOX (PDF)

■ AUTHOR INFORMATION

Corresponding Authors

Ding-Shyue Yang − *Department of Chemistry, University of Houston, Houston, Texas 77204, United States;* orcid.org/0000-0003-2713-9128; Email: yang@uh.edu

Thalappil Pradeep − *DST Unit of Nanoscience (DST UNS) and Thematic Unit of Excellence (TUE), Department of Chemistry, Indian Institute of Technology Madras, Chennai 600036, India; International Centre for Clean Water, Chennai 600113, India;* orcid.org/0000-0003-3174-534X; Email: pradeep@iitm.ac.in

Author

Bijesh K. Malla − *DST Unit of Nanoscience (DST UNS) and Thematic Unit of Excellence (TUE), Department of Chemistry, Indian Institute of Technology Madras, Chennai 600036, India*

Complete contact information is available at: https://pubs.acs.org/10.1021/acs.jpclett.4c03106

Author Contributions

Thalappil Pradeep, Ding-Shyue Yang, and Bijesh K. Malla designed the research. Ding-Shyue Yang and Bijesh K. Malla have performed the experiments and analyzed the results. Thalappil Pradeep and Ding-Shyue Yang supervised the progress. The manuscript was prepared with contributions from all authors.

Notes

The authors declare no competing financial interest.

■ ACKNOWLEDGMENTS

The authors acknowledge the Science and Engineering Research Board (SERB), Department of Science and Technology (DST), and Government of India for research funding. Thalappil Pradeep acknowledges funding from the Centre of Excellence on Molecular Materials and Functions under the Institution of Eminence Scheme of Indian Institute of Technology (IIT) Madras. Ding-Shyue Yang acknowledges the support of the National Science Foundation (CHE-2154363). Bijesh K. Malla thanks the Council of Scientific and Industrial Research (CSIR) for his research fellowship. Bijesh K. Malla was a recipient of the International Immersion Experience (IIE) travel fellowship of IIT Madras.

■ REFERENCES

(1) Ghosh, J.; Vishwakarma, G.; Kumar, R.; Pradeep, T. Formation and Transformation of Clathrate Hydrates under Interstellar Conditions. *Acc. Chem. Res.* **2023**, *56* (16), 2241−2252.

(2) Sloan, E. D., Jr.; Koh, C. A. Introduction: Clathrate Hydrates of Natural Gases. *Clathrate Hydrates of Natural Gases*; CRC Press: Boca Raton, FL, 2008; pp I−XXV.

(3) Sloan, E. D., Jr.; Koh, C. A. *Clathrate Hydrates of Natural Gases*; CRC Press: Boca Raton, FL, 2007; DOI: 10.1201/9781420008494.

(4) Chong, Z. R.; Yang, S. H. B.; Babu, P.; Linga, P.; Li, X.-S. Review of Natural Gas Hydrates as an Energy Resource: Prospects and Challenges. *Appl. Energy* **2016**, *162*, 1633−1652.

(5) Khurana, M.; Yin, Z.; Linga, P. A Review of Clathrate Hydrate Nucleation. *ACS Sustainable Chem. Eng.* **2017**, *5* (12), 11176−11203.

(6) Ghosh, J.; Methikkalam, R. R. J.; Bhuin, R. G.; Ragupathy, G.; Choudhary, N.; Kumar, R.; Pradeep, T. Clathrate Hydrates in Interstellar Environment. *Proc. Natl. Acad. Sci. U. S. A.* **2019**, *116* (5), 1526−1531.

(7) Malla, B. K.; Vishwakarma, G.; Chowdhury, S.; Selvarajan, P.; Pradeep, T. Formation of Ethane Clathrate Hydrate in Ultrahigh Vacuum by Thermal Annealing. *J. Phys. Chem. C* **2022**, *126* (42), 17983−17989.

(8) Ghosh, J.; Vishwakarma, G.; Das, S.; Pradeep, T. Facile Crystallization of Ice Ihvia Formaldehyde Hydrate in Ultrahigh Vacuum under Cryogenic Conditions. *J. Phys. Chem. C* **2021**, *125* (8), 4532−4539.

(9) Ghosh, J.; Bhuin, R. G.; Vishwakarma, G.; Pradeep, T. Formation of Cubic Ice via Clathrate Hydrate, Prepared in Ultrahigh Vacuum under Cryogenic Conditions. *J. Phys. Chem. Lett.* **2020**, *11* (1), 26−32.

(10) Vishwakarma, G.; Malla, B. K.; Chowdhury, S.; Khandare, S. P.; Pradeep, T. Existence of Acetaldehyde Clathrate Hydrate and Its Dissociation Leading to Cubic Ice under Ultrahigh Vacuum and Cryogenic Conditions. *J. Phys. Chem. Lett.* **2023**, *14*, 5328−5334.

(11) Ghosh, J.; Bhuin, R. G.; Ragupathy, G.; Pradeep, T. Spontaneous Formation of Tetrahydrofuran Hydrate in Ultrahigh Vacuum. *J. Phys. Chem. C* **2019**, *123* (26), 16300−16307.

(12) Vishwakarma, G.; Malla, B. K.; Reddy, K. S. S. V. P.; Ghosh, J.; Chowdhury, S.; Yamijala, S. S. R. K. C.; Reddy, S. K.; Kumar, R.; Pradeep, T. Induced Migration of CO_2 from Hydrate Cages to Amorphous Solid Water under Ultrahigh Vacuum and Cryogenic Conditions. *J. Phys. Chem. Lett.* **2023**, *14*, 2823−2829.

(13) Malla, B. K.; Vishwakarma, G.; Chowdhury, S.; Nayak, S. K.; Yamijala, S. S. R. K. C.; Pradeep, T. Formation and Dissociation of Dimethyl Ether Clathrate Hydrate in Interstellar Ice Mimics. *J. Phys. Chem. C* **2024**, *128* (6), 2463−2470.

(14) Blake, D.; Allamandola, L.; Sandford, S.; Hudgins, D.; Freund, F. Clathrate Hydrate Formation in Amorphous Cometary Ice Analogs in Vacuo. *Science* **1991**, *254* (5031), 548−551.

(15) Fleyfel, F.; Devlin, J. P. Carbon Dioxide Clathrate Hydrate Epitaxial Growth: Spectroscopic Evidence for Formation of the Simple Type-II CO_2 Hydrate. *J. Phys. Chem.* **1991**, *95* (9), 3811−3815.

(16) Ramakrishnan, S.; Sagi, R.; Mahapatra, N.; Asscher, M. Effect of Coadsorbed Oxygen on the Photochemistry of Methane Embedded in Amorphous Solid Water. *J. Phys. Chem. C* **2018**, *122* (27), 15287−15296.

(17) Ayoub, Y.; Asscher, M. Interaction of Ethyl Chloride with Amorphous Solid Water Thin Film on Ru(00l) and O/Ru(00l) Surfaces. *J. Phys. Chem. A* **2009**, *113* (26), 7514−7520.
(18) Horowitz, Y.; Asscher, M. Electron-Induced Chemistry of Methyl Chloride Caged within Amorphous Solid Water. *J. Chem. Phys.* **2013**, *139* (15), No. 154707.
(19) Souda, R.; Aizawa, T. Reflection High Energy Electron Diffraction (RHEED) Study of Ice Nucleation and Growth on Ni(111): Influences of Adspecies and Electron Irradiation. *Phys. Chem. Chem. Phys.* **2019**, *21* (35), 19585−19593.
(20) Souda, R.; Aizawa, T.; Sugiyama, N.; Takeguchi, M. Structure Analysis of Water Ice Crystallites on NaCl(001), KCl(001), and CaF_2(111) by Reflection High-Energy Electron Diffraction. *J. Phys. Chem. C* **2020**, *124* (28), 15180−15187.
(21) Yang, D. S.; Zewail, A. H. Ordered Water Structure at Hydrophobic Graphite Interfaces Observed by 4D, Ultrafast Electron Crystallography. *Proc. Natl. Acad. Sci. U. S. A.* **2009**, *106* (11), 4122−4126.
(22) Minissale, M.; Aikawa, Y.; Bergin, E.; Bertin, M.; Brown, W. A.; Cazaux, S.; Charnley, S. B.; Coutens, A.; Cuppen, H. M.; Guzman, V.; Linnartz, H.; McCoustra, M. R. S.; Rimola, A.; Schrauwen, J. G. M.; Toubin, C.; Ugliengo, P.; Watanabe, N.; Wakelam, V.; Dulieu, F. Thermal Desorption of Interstellar Ices: A Review on the Controlling Parameters and Their Implications from Snowlines to Chemical Complexity. *ACS Earth Space Chem.* **2022**, *6* (3), 597−630.
(23) Yang, D.-S.; He, X. Structures and Ultrafast Dynamics of Interfacial Water Assemblies on Smooth Hydrophobic Surfaces. *Chem. Phys. Lett.* **2017**, *683*, 625−632.
(24) He, X.; Wu, C.; Rajagopal, K.; Punpongjareorn, N.; Yang, D. S. Ordered Ionic Liquid Structure Observed at Terraced Graphite Interfaces. *Phys. Chem. Chem. Phys.* **2016**, *18* (5), 3392−3396.
(25) Wu, C.; Yang, D. S. Ordered Structures and Morphology-Induced Phase Transitions at Graphite-Acetonitrile Interfaces. *J. Phys. Chem. C* **2019**, *123* (36), 22390−22396.
(26) He, X.; Wu, C.; Yang, D.-S. Communication: No Guidance Needed: Ordered Structures and Transformations of Thin Methanol Ice on Hydrophobic Surfaces. *J. Chem. Phys.* **2016**, *145* (17), 171102.
(27) He, X.; Yang, D. S. Order-Determined Structural and Energy Transport Dynamics in Solid-Supported Interfacial Methanol. *Nano Lett.* **2021**, *21* (3), 1440−1445.
(28) He, X.; Yang, D. S. Ethanol on Graphite: Ordered Structures and Delicate Balance of Interfacial and Intermolecular Forces. *J. Phys. Chem. C* **2021**, *125* (43), 24145−24154.
(29) Snyder, L. E.; Buhl, D.; Schwartz, P. R.; Clark, F. O.; Johnson, D. R.; Lovas, F. J.; Giguere, P. T. Radio Detection of Interstellar Dimethyl Ether. *Astrophys. J.* **1974**, *191*, L79.
(30) McGuire, B. A.; Carroll, P. B.; Loomis, R. A.; Finneran, I. A.; Jewell, P. R.; Remijan, A. J.; Blake, G. A. Detection of Interstellar Ethylene Oxide (c-C_2H_4O). *Science* **2016**, *352* (6292), 1449−1452.
(31) McGuire, B. A.; Carroll, P. B.; Loomis, R. A.; Finneran, I. A.; Jewell, P. R.; Remijan, A. J.; Blake, G. A. Discovery of the Interstellar Chiral Molecule Propylene Oxide (CH_3CHCH_2O). *Science* **2016**, *352* (6292), 1449−1452.
(32) Cyriac, J.; Pradeep, T.; Kang, H.; Souda, R.; Cooks, R. G. Low-Energy Ionic Collisions at Molecular Solids. *Chem. Rev.* **2012**, *112* (10), 5356−5411.
(33) Kang, H. Chemistry of Ice Surfaces. Elementary Reaction Steps on Ice Studied by Reactive Ion Scattering. *Acc. Chem. Res.* **2005**, *38* (12), 893−900.
(34) Jenniskens, P.; Blake, D. F. Structural Transitions in Amorphous Water Ice and Astrophysical Implications. *Science* **1994**, *265* (5173), 753−756.
(35) Dobrzycki, L.; Taraszewska, P.; Boese, R.; Cyrański, M. K. Pyrrolidine and Its Hydrates in the Solid State. *Cryst. Growth Des.* **2015**, *15* (10), 4804−4812.
(36) Dowell, L. G.; Rinfret, A. P. Low-Temperature Forms of Ice as Studied by X-Ray Diffraction. *Nature* **1960**, *188* (4757), 1144−1148.
(37) Momma, K.; Izumi, F. VESTA 3 for Three-Dimensional Visualization of Crystal, Volumetric and Morphology Data. *J. Appl. Crystallogr.* **2011**, *44* (6), 1272−1276.
(38) Huang, X.; Wang, L.; Liu, K.; Liao, L.; Sun, H.; Wang, J.; Tian, X.; Xu, Z.; Wang, W.; Liu, L.; Jiang, Y.; Chen, J.; Wang, E.; Bai, X. Tracking Cubic Ice at Molecular Resolution. *Nature* **2023**, *617* (7959), 86−91.
(39) Lee, M.; Lee, S. Y.; Kang, M.-H.; Won, T. K.; Kang, S.; Kim, J.; Park, J.; Ahn, D. J. Observing Growth and Interfacial Dynamics of Nanocrystalline Ice in Thin Amorphous Ice Films. *Nat. Commun.* **2024**, *15* (1), 908.
(40) Hong, J.; Tian, Y.; Liang, T.; Liu, X.; Song, Y.; Guan, D.; Yan, Z.; Guo, J.; Tang, B.; Cao, D.; Guo, J.; Chen, J.; Pan, D.; Xu, L. M.; Wang, E. G.; Jiang, Y. Imaging Surface Structure and Premelting of Ice Ih with Atomic Resolution. *Nature* **2024**, *630* (8016), 375−380.
(41) Park, J. S.; Noh, N.; Park, J.; Shim, Y.; Park, S.; Qureshi, Y.; Kang, S.; Huh, Y.; Lee, C.-W.; Yuk, J. M. Phase Transition of Cubic Ice to Hexagonal Ice during Growth and Decomposition. *Nano Lett.* **2024**, *24* (37), 11504−11511.
(42) Dowell, L. G.; Rinfret, A. P. Low-Temperature Forms of Ice as Studied by X-Ray Diffraction. *Nature* **1960**, *188* (4757), 1144−1148.
(43) Sargent, D. F.; Calvert, L. D. Crystallographic Data for Some New Type II Clathrate Hydrates. *J. Phys. Chem.* **1966**, *70* (8), 2689−2691.
(44) Ghosh, M.; Yang, D.-S. Structures of Self-Assembled n -Alkanethiols on Gold by Reflection High-Energy Electron Diffraction. *Phys. Chem. Chem. Phys.* **2020**, *22* (30), 17325−17335.
(45) Andersson, O.; B. Brant Carvalho, P. H.; Haussermann, U.; Hsu, Y.-J. Evidence Suggesting Kinetic Unfreezing of Water Mobility in Two Distinct Processes in Pressure-Amorphized Clathrate Hydrates. *Phys. Chem. Chem. Phys.* **2022**, *24* (34), 20064−20072.
(46) Guo, G.-J.; Zhang, Z. Open Questions on Methane Hydrate Nucleation. *Commun. Chem.* **2021**, *4* (1), 1−3.
(47) Li, L.; Zhong, J.; Yan, Y.; Zhang, J.; Xu, J.; Francisco, J. S.; Zeng, X. C. Unraveling Nucleation Pathway in Methane Clathrate Formation. *Proc. Natl. Acad. Sci. U. S. A.* **2020**, *117* (40), 24701−24708.
(48) Jacobson, L. C.; Hujo, W.; Molinero, V. Amorphous Precursors in the Nucleation of Clathrate Hydrates. *J. Am. Chem. Soc.* **2010**, *132* (33), 11806−11811.

https://doi.org/10.1021/acs.jpclett.4c03106
J. Phys. Chem. Lett. 2025, 16, 365−371